

Multi-HMR: Multi-Person Whole-Body Human Mesh Recovery in a Single Shot

Fabien Baradel* Matthieu Armando Salma Galaaoui Romain Brégier
Philippe Weinzaepfel Grégory Rogez Thomas Lucas*

NAVER LABS Europe

*equal contribution

<https://github.com/naver/multi-hmr>

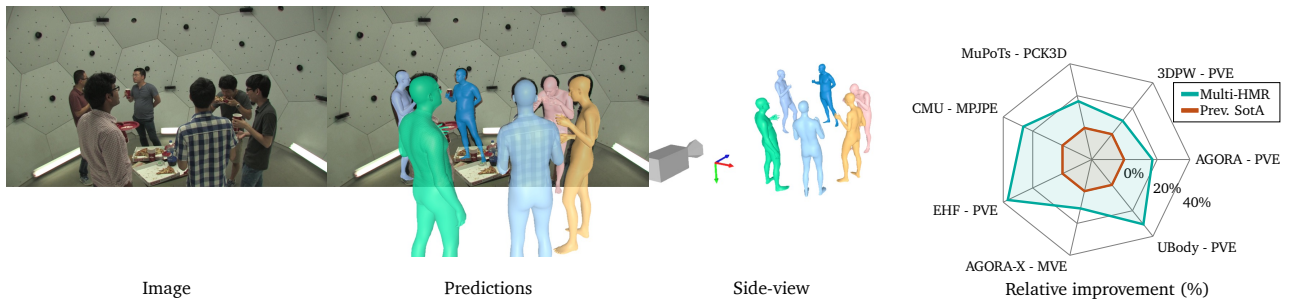


Figure 1: **Efficient 3D reconstruction of multiple humans in camera space.** We introduce Multi-HMR, a single-shot approach to detect *multiple humans*, regress *whole-body* human meshes that capture faces and hands and place them in the scene. *Left*: Visualization of Multi-HMR predictions. *Right*: Relative improvements (in %) on human mesh recovery benchmarks.

Abstract

We present Multi-HMR, a strong single-shot model for *multi-person* 3D human mesh recovery from a single RGB image. Predictions encompass the *whole body*, *i.e.*, including hands and facial expressions, using the SMPL-X parametric model and *spatial location* in the camera coordinate system. Our model detects people by predicting coarse 2D heatmaps of person centers, using features produced by a standard Vision Transformer (ViT) backbone. It then predicts their whole-body pose, shape and spatial location using a new cross-attention module called the Human Prediction Head (HPH), with one query per detected center token, attending to the entire set of features. As direct prediction of SMPL-X parameters yields suboptimal results, we introduce CUFFS; the Close-Up Frames of Full-Body Subjects dataset, containing humans close to the camera with diverse hand poses. We show that incorporating this dataset into training further enhances predictions, particularly for hands, enabling us to achieve state-of-the-art performance. Multi-HMR also optionally accounts for *camera intrinsics*, if available, by encoding camera ray directions for each image token. This simple design achieves strong performance on whole-body and body-only benchmarks simultaneously. We train models with various backbone sizes and input resolutions. In particular, using a ViT-S backbone and 448×448 input images already yields a fast and competitive model with respect to state-of-the-art methods, while considering larger models and higher resolutions further improve performance.

1. Introduction

We introduce a single-shot model for recovering whole-body 3D meshes of humans from a single RGB image. Our problem formulation focuses on four aspects of Human Mesh Recovery (HMR) that we identify as pivotal to making HMR applicable to real-world scenarios: i) capture of expressive body poses – *i.e.*, including faces

and hands, ii) efficient processing of a variable number of people, iii) spatial location of the humans in camera space, iv) adaptability to camera information if available.

Successfully handling these aspects simultaneously makes our proposed model, denoted Multi-HMR, widely applicable. For instance, in virtual or augmented

Method		Whole Body	Single Shot	Camera Space	Camera Aware
Single-person	HMR [23]	✗	✓	✗	✗
	HMR2.0 [13]	✗	✓	✗	✗
	SPEC [25]	✗	✓	✗	✓
	CLIFF [27]	✗	✓	✗	✓
	PIXIE [12]	✓	✗	✗	✗
	Hand4Whole [39]	✓	✗	✗	✗
	OSX [28]	✓	✗	✗	✗
Det. + Single	3DCrowdNet [7]	✗	✗	✗	✗
	ROMP [53]	✗	✓	✗	✗
Multi-person	BEV [54]	✗	✓	✓	✗
	PSVT [45]	✗	✓	✓	✗
	Multi-HMR	✓	✓	✓	Optional

Table 1: **Main features** of Multi-HMR vs. the state-of-the-art methods: Single-person methods rely on human detectors followed by crops around each person. Multi-person approaches detect humans and regress their properties using the same network. ‘Single-shot’ refers to methods that directly regress the expected output without extracting or resampling features from different crops.

reality (AR/VR), capturing faces and hands precisely is key as it is an important component of human communication. It is also beneficial for enabling human-robot interactions [9, 51], or human understanding from images and videos [47, 52, 66].

Likewise, understanding the placement of people in the scene is necessary for applications ranging from robotic navigation to AR/VR applications involving several people. In addition, efficient processing of a variable number of people is desirable when computation is restricted or real-time processing is needed. Finally, reasoning about 3D meshes can only benefit from adapting to camera information when it is available [25, 27].

In their pioneering work on HMR [23], Kanazawa *et al.* propose to predict SMPL mesh parameters and three parameters for weak-perspective reprojection given a cropped image containing a person. Different aspects of this approach have been improved since, including architectures [13, 27, 63], training techniques [26] and data enhancements [5, 22, 42]. The approach has also been extended to whole-body parametric models like SMPL-X [43], often with multiple crops centered on body, hands and face [8, 12, 39]. Multi-person inputs are typically handled with a two-step procedure: first running an off-the-shelf human detector, then applying a mesh recovery model on crops around each detected person. Conversely, ROMP [53] and PSVT [45] recover multiple human meshes in a single step using one-shot detectors. BEV [54] additionally predicts the relative depths of meshes. Accounting for intrinsic camera parameters has been shown to improve reprojection [25,

27], especially when these differ between training and inference. Despite these advancements, no previous method has successfully integrated in a single model all four essential features, see Figure 1 (left): efficient multi-person processing, whole-body mesh recovery, location estimation in camera space and, optionally, camera-aware predictions (see Table 1).

In this paper, we introduce Multi-HMR, an efficient single-shot detector that regresses pose and shape parameters of a whole-body parametric model, for each person in the scene, and places the predicted 3D meshes in camera space. Optionally, it can be conditioned on camera intrinsics if available. Figure 2 presents an overview of the model architecture. To extract features from the input data, we utilize a standard Vision Transformer (ViT) [10] backbone, which allows us to benefit from recent advancements in large-scale self-supervised pre-training [6, 16, 41]. This differs from architectures like HR-Net which are less standard in the pre-training literature. Following the CenterNet object detection framework [67], we regress a person-center heatmap from the feature tensor produced by the backbone: for each input token, the model first outputs a probability that a person is centered on a point present in the corresponding input patch, as well as location offsets. We introduce a prediction head called the Human Perception Head (HPH) that employs cross-attention. In this mechanism, queries correspond to the detected center token, while keys and values are drawn from all image tokens. It efficiently predicts a variable number of pose and shape parameters for an expressive human parametric model, namely SMPL-X [8], while also determining depths for accurate placement of individuals within the scene. To improve 3D prediction by incorporating camera intrinsics, our model can optionally take camera parameters as input. These parameters are utilized to augment each token feature with Fourier-encoding of the corresponding camera ray directions before passing them to the prediction head.

Multi-HMR is conceptually simple: unlike many existing approaches, it does not rely on multiple high-resolution crops of the body parts for expressive models [8, 12, 39], or hand-designed components to place people in the scene [7, 53]. However, naively regressing SMPL-X parameters from a single token tends to perform low on small body parts such as hands. We find that incorporating expressive human subjects positioned close to the cameras in the training data results in good performance across all body parts. To achieve this, we introduce CUFFS, the Close-Up Frames of Full-Body Subjects dataset, containing synthetic renderings of people with clearly visible hands in diverse poses.

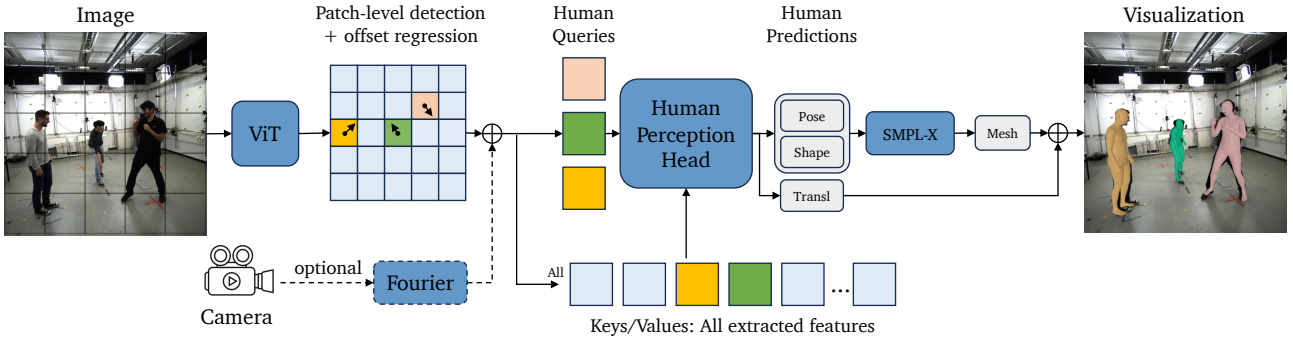


Figure 2: **Overview of Multi-HMR.** A ViT backbone extracts image embeddings. Detection is conducted at the patch level and includes an additional 2D offset regression. Each detected token feature serves as a query for a cross-attention based head, called Human Perception Head, which predicts pose and shape parameters, along with spatial location in 3D space. Optionally, if camera parameters are known, a camera embedding is added for each patch, represented as a Fourier encoding of the ray originating from the camera center.

We train different models with various backbone sizes and input resolutions. We evaluate performance on several benchmarks, see Figure 1 (Right): both body-only mesh recovery datasets (3DPW [57], MuPoTs [32], CMU-Panoptic [21], AGORA-SMPL [42]) and whole-body mesh recovery datasets (EHF [43], AGORA-SMPLX [42] and UBody [28]). The single-shot nature of the model allows for efficient inference. For instance, with a ViT-S backbone and 448×448 inputs, Multi-HMR is competitive on both body-only and whole-body benchmarks while allowing for real-time applications with 30 frames per second (fps). Larger backbones and higher resolution – up to a ViT-L backbone and 896×896 inputs – further improve performance at the cost of slower but still reasonable inference (5 fps).

2. Related work

Multi-HMR primarily builds upon whole-body HMR and multi-person HMR. It also relies on synthetic datasets. We now review these three literatures.

Whole-body Human Mesh Recovery. There has been a recent surge of interest for whole-body mesh recovery from a single image [12, 28, 39, 43], fostered in part by seminal work on improving whole-body parametric models. In particular SMPL-X [43] outputs an expressive mesh for the whole body given a small set of pose and shape parameters. The first approaches were based on optimization, *e.g.* SMPLify-X [43], but they remain slow and sensitive to local minima. Numerous learning-based methods were also introduced, but only in single-person settings [8, 12, 39, 50, 68]. This setting already poses significant challenges: hands and faces are typically low resolution in natural images, and capturing their poses hinges on subtle details. To overcome this, most approaches leverage a multi-crop pipeline: areas of interest – such as the face and

hands – are cropped, resized and used to estimate the associated meshes which are aggregated into a whole-body prediction. In particular, ExPose [8] selects high-resolution crops using a body-driven attention mechanism; PIXIE [12] fuses body parts in an adaptive manner, and Hand4Whole [39] uses both body and hand joint features for 3D wrist rotation estimation. In contrast to these methods, Multi-HMR is single-shot, without high-resolution crops. More recently, OSX [28] introduced the first single-crop method for single-person whole-body mesh recovery. They leverage a ViT encoder, followed by a high-resolution feature pyramid, and use keypoint (*e.g.* wrists) estimates to resample features in their decoder head. We depart from existing methods by i) tackling *multi-person* whole-body mesh recovery and ii) using a single-shot approach, with a non-hierarchical feature extractor.

Multi-Person Human Mesh Recovery. Most existing multi-person HMR methods [7, 13, 26, 44, 63] build upon a multi-stage framework: an off-the-shell human detector [15, 30, 48] is used, followed by a single-person mesh estimation model [24, 31, 62, 65] to process each detected human. This has two drawbacks: i) it is inefficient at inference time compared to a single-shot approach and ii) the pipeline cannot be learned end-to-end. This impacts final performance, in particular in cases of truncation by the image frame or person-person occlusions, a common scenario in multi-person settings. Following the seminal work of ROMP [53] which estimates 2D maps for 2D human detections, positions and mesh parameters, single-stage models have been proposed [45, 53, 54]. In particular, BEV [54] introduces an additional Bird-Eye-View representation of the scene to predict relative depth between detected persons and PSVT [45] improves performance using a transformer decoder. We follow the same single-shot philosophy as [45, 53, 54] but go beyond their settings

by: i) tackling whole-body mesh recovery, ii) regressing the 3D spatial location of each person in the camera coordinate system, and iii) incorporating camera intrinsics as an optional input to the model to further improve accuracy. We also introduce an efficient cross-attention-based head, making Multi-HMR faster to train, efficient at inference and capable of achieving improved performance.

Synthetic data. Acquiring high-quality real-world ground-truth data at scale for human mesh recovery is costly, in particular when considering faces and hands. A body of work [14, 56, 61] has explored the generation of large-scale synthetic data for human-related tasks. In this work, we experiment with BEDLAM [5] and AGORA [42], and confirm empirically that using large-scale synthetic data is beneficial for whole-body human mesh regression, compared to real-world data with pseudo ground-truth fits. We also propose a new synthetic dataset, CUFFS, which stands for Close-Up Frames of Full-Body Subjects, designed to improve performance particularly on hands for one-stage whole-body prediction. It departs from existing ones in that it contains diverse and clearly visible hand poses, seen from a limited distance, to allow fine details to be captured. Our experiments show that this type of training data is key to allow regressing whole-body meshes in a single shot.

3. Multi-HMR

We now describe our single-shot multi-person whole-body human mesh recovery approach. Given an input RGB image $\mathbf{I} \in \mathbb{R}^{H \times W \times 3}$ with resolution $H \times W$, our model, denoted \mathcal{H} , directly outputs a set of N centered whole-body 3D humans meshes $\mathbf{M} \in \mathbb{R}^{V \times 3}$ (composed of V vertices), along their corresponding with 3D spatial locations $\mathbf{t} \in \mathbb{R}^3$ in the camera coordinate system:

$$\{\mathbf{M}_n + \mathbf{t}_n\}_{n \in \{1, \dots, N\}} = \mathcal{H}(\mathbf{I}). \quad (1)$$

As preliminaries, Section 3.1 presents the 3D whole-body parametric model and the camera model that we use. We then detail the model architecture in Section 3.2 and the training losses in Section 3.3.

3.1. Preliminaries

Human whole-body mesh representation. We build upon the parametric 3D body model SMPL-X [8]. Given input parameters for the pose $\boldsymbol{\theta} \in \mathbb{R}^{53 \times 3}$ (global orientation, body, hands and jaw poses) expressed using axis-angle representation, shape $\boldsymbol{\beta} \in \mathbb{R}^{10}$ and facial expression $\boldsymbol{\alpha} \in \mathbb{R}^{10}$, it outputs an expressive human-

centered 3D mesh $\mathbf{M} = \text{SMPL-X}(\boldsymbol{\theta}, \boldsymbol{\beta}, \boldsymbol{\alpha}) \in \mathbb{R}^{V \times 3}$, with $V = 10475$ vertices. The mesh \mathbf{M} is centered around a *primary* keypoint – the pelvis is often used, but in this work we choose the head as primary keypoint. It is placed in the 3D scene by translating the primary keypoint by a 3D translation \mathbf{t} . For the sake of simplicity, let $\mathbf{x} = [\boldsymbol{\theta}, \boldsymbol{\beta}, \boldsymbol{\alpha}]$: the problem reduces to predicting \mathbf{x} and \mathbf{t} for all detected humans.

Pinhole camera model. We assume a simple pinhole camera model to project 3D points on the image plane. Ignoring distortion, it is defined by an intrinsic matrix $\mathbf{K} \in \mathbb{R}^{3 \times 3}$ of focal length f and principal point (p_u, p_v) . We set the camera pose to the origin. Let $\mathbf{t} = (t_x, t_y, t_z)$ be a 3D point. We have:

$$\mathbf{K} = \begin{bmatrix} f & 0 & p_u \\ 0 & f & p_v \\ 0 & 0 & 1 \end{bmatrix} \quad \text{and} \quad \begin{cases} [c_u, c_v, 1]^T = (1/t_z) \cdot \mathbf{K} [t_x, t_y, t_z]^T \\ [t_x, t_y, t_z]^T = t_z \cdot \mathbf{K}^{-1} [c_u, c_v, 1]^T, \end{cases} \quad (2)$$

with $\mathbf{c} = (c_u, c_v)$ the 2D image coordinates of the projection of \mathbf{t} into the image plane. \mathbf{K} can thus be used to backproject a 2D point into 3D given its depth t_z . We denote by $\pi_{\mathbf{K}}$ the camera projection operator and $\pi_{\mathbf{K}}^{-1}$ the camera inverse projection operator.

3.2. Single-shot architecture

Our method is summarized in Figure 2. We first encode images into token embeddings using a ViT backbone. These embeddings are used to detect humans and can optionally be combined with camera embeddings. Our proposed Human Perception Head is then employed to regress whole-body human meshes and depth for a variable number of detected humans.

ViT backbones. The input RGB image \mathbf{I} is encoded with a ViT backbone [10]. It is sub-divided into image patches of size $P \times P$, each embedded into tokens with a linear transformation and positional encoding. The set of tokens is processed with self-attention blocks into $\mathbf{E} \in \mathbb{R}^{H/P \times W/P \times D}$ with D the feature dimension. The ViT model keeps a constant resolution throughout so that each output token spatially corresponds to a patch in the input image.

Patch-level detection. To detect humans in the input image, we follow the CenterNet [67] paradigm. We define a *primary keypoint* on human bodies, here the 3D keypoint of the *head* as defined according to the SMPL-X body model. For each patch index $(i, j) \in \{1, \dots, H/P\} \times \{1, \dots, W/P\}$, we predict if the patch centered at $\mathbf{u}^{i,j} = (u^i, v^j)$ contains a primary keypoint, with a score $s^{i,j} \in [0, 1]$ computed from the associated token embedding $\mathbf{E}^{i,j} \in \mathbb{R}^D$ using a Multi-Layer-Peceptor (MLP). At inference, we apply a threshold τ to the scores

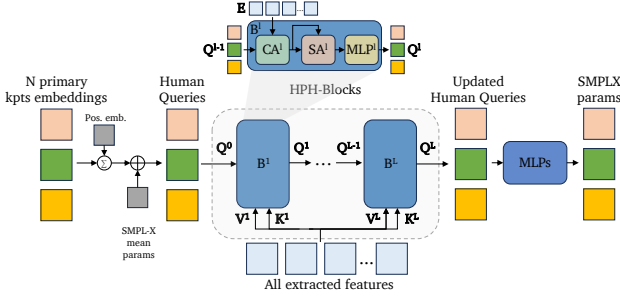


Figure 3: **Human Perception Head.** The token embeddings corresponding to the N detected primary keypoints are updated by using them as queries in a series of cross-attention blocks where keys and values correspond to the context provided by all tokens. MLPs then predict the SMPL-X parameters (pose and shape) as well as the depth for each query.

to detect patches containing primary keypoints:

$$\{\mathbf{u}_n\}_n = \{\mathbf{u}^{i,j} | s^{i,j} \geq \tau\}. \quad (3)$$

At train time, the ground-truth detections are used for the rest of the model.

Image coordinates regression. Detecting people at the patch level yields a rough estimation of the 2D location of the primary keypoint, up to the size of the predefined patch size P . We refine the 2D location of the primary keypoint from the center of a patch (u^i, v^j) by regressing a residual offset $\delta = (\delta_u, \delta_v)$ from the corresponding token embedding $\mathbf{E}^{i,j}$ using an MLP. The final pixel coordinates of the primary keypoint detected at patch location (i, j) is given by :

$$\mathbf{c}^{i,j} = [u^i + \delta_u, v^j + \delta_v]. \quad (4)$$

Human Perception Head (HPH). We predict a variable number of human-centered meshes and depths for all people detected in the scene in a structured manner and in parallel, by processing \mathbf{E} with our Human Perception Head, built from cross-attention blocks [19], see Figure 3 for an overview. This design choice allows features corresponding to a person detection to attend information from all image patches before making a full pose, shape and depth prediction for this person. Given N detected humans, we initialize N cross-attention queries $\{\mathbf{q}_n\}_n$. Assuming \mathbf{q}_n was detected at patch (i, j) , $\mathbf{q}_n = (\mathbf{E}^{i,j} \oplus \bar{\mathbf{x}}) + \mathbf{p}^{i,j}$ where $\mathbf{p}^{i,j}$ is a learned query initialization, dependent on position, and $\bar{\mathbf{x}}$ denotes the mean body model parameters, of dimension D' , as in previous works [13, 26]. The queries are stacked into $\mathbf{Q}^0 \in \mathbb{R}^{(D+D') \times N}$ for efficient processing in parallel. The full feature tensor \mathbf{E} is used as cross-attention keys and values. The queries are then updated

with a stack of L blocks \mathbf{B}^l ($L=2$ in practice), alternating between cross-attention layers (CA) over queries and image features, and self-attention layers (SA) over queries and a top-head MLP :

$$\mathbf{Q}^l = \mathbf{B}^l [\mathbf{Q}^{l-1}, \mathbf{E}] = \text{MLP}^l \left(\text{SA}^l \left(\text{CA}^l [\mathbf{Q}^{l-1}, \mathbf{E}] \right) \right). \quad (5)$$

The final outputs of the cross-attention based module are given by $\mathbf{Q}^L \in \mathbb{R}^{(D+D') \times N}$ and viewed as a set of N output features, used to regress N human-centered whole-body parameters $\{\mathbf{x}_n\}_n$ with a shared MLP.

Depth parametrization. As is standard in the monocular depth literature [34, 59], we predict the depth d in log-space (also called *nearness* [46] denoted η). We regress a *normalized* nearness $\hat{\eta}$ from \mathbf{Q}^L using an MLP, assuming a *standard* focal length \hat{f} :

$$\begin{cases} \eta &= \frac{\hat{f}}{f} \hat{\eta}, \\ d &= \exp(-\eta). \end{cases} \quad (6)$$

This follows [11] which shows that this parametrization improves robustness to focal length changes. The depth d is used to back-project the 2D camera coordinates \mathbf{c} using the camera inverse projection operator $\pi_{\mathbf{K}}^{-1}$ following Equation 2 to obtain the 3D translation \mathbf{t} of the primary keypoint.

We want to highlight that we directly supervise the *absolute* depth while most previous works [54] supervise the *relative* depth. This is made possible by the utilization of large-scale synthetic data, where absolute depth can be determined, as opposed to real-world data where only relative depth can be annotated. Our experimental results show that this simple strategy is effective.

Optional camera embedding. If available, camera intrinsics \mathbf{K} can be used as additional input to our model \mathcal{H} which becomes $\mathcal{H}(\mathbf{I}, \mathbf{K})$. In more details, camera information may be integrated into the Human Perception Head at training and/or inference time. This is a desirable feature, but making it optional allows for i) processing images when it is not available; and ii) fairly comparing to state-of-the-art methods that do not use this information.

We embed camera information by computing the ray direction [36] $\mathbf{r}_{i,j} = \mathbf{K}^{-1}[u_i, v_j, 1]^T$ from each patch center (u_i, v_j) . The first two values of the $\mathbf{r}_{i,j}$ vector are kept, and embedded into a high-dimensional space using Fourier encoding [36] to obtain a patch-level geometric embedding $\mathbf{E}_{\mathbf{K}} \in \mathbb{R}^{H/P \times W/P \times 2(F+1)}$, where F is the number of frequency bands. We concatenate features extracted using the vision backbone with camera embeddings to update them and get $\mathbf{E} \doteq \mathbf{E} \oplus \mathbf{E}_{\mathbf{K}}$, where \oplus denotes concatenation along the channel axis.

Backbone	Head	MuPoTs \uparrow	3DPW \downarrow	EHF \downarrow	CMU \downarrow
HRNet	Reg	65.8	83.2	143.1	130.1
ViT-S	Reg	70.1	80.2	90.6	118.1
HRNet	HPH	69.8	80.2	115.2	116.6
ViT-S	HPH	70.9	80.1	80.1	109.1
ViT-B	HPH	76.3	73.5	55.3	97.2

(a) Architecture

Data	MuPoTs \uparrow	3DPW \downarrow	EHF \downarrow	EHF-H \downarrow	CMU \downarrow
Real	68.5	83.8	70.2	51.2	101.6
A+B	76.3	73.5	55.3	47.4	97.2
A+B+C	76.0	72.9	49.8	40.5	96.5
+Real	69.8	77.6	61.1	48.4	98.5

‘A’=AGORA, ‘B’=BEDLAM, and ‘C’=CUFFS

(b) Data

Table 2: **Ablation on the architecture and training data** on MuPoTs (PCK3D-All), 3DPW (MPJPE), EHF (PVE-All), EHF-H (PVE-Hands) and CMU (MPJPE). Default settings in grey. (a) We compare a ViT backbone to HRNet as well as our HPH with respect to a standard iterative regressor [23] ‘Reg’. (b) Training data type; ‘Real’ corresponds to MS-CoCo, MPII and Human 3.6M.

3.3. Training Multi-HMR

Multi-HMR is fully-differentiable and trained end-to-end by back-propagation. We now discuss training losses. $A \sim$ denotes ground-truth targets.

Detection loss. We project the ground-truth primary keypoint of each human present in the image using the camera projection operator π_K , and construct a score map \tilde{S} of dimension $(W/P) \times (H/P)$ with $S^{i,j}$ equal to 1 if a primary keypoint is projected to the corresponding patch and 0 otherwise. Predictions are trained by minimizing a binary cross-entropy loss:

$$\mathcal{L}_{\text{det}} = - \sum_{i,j} \tilde{s}^{i,j} \log(s^{i,j}) + (1 - \tilde{s}^{i,j}) \log(1 - s^{i,j}). \quad (7)$$

Regression losses. All other quantities predicted by the model are trained with L_1 regression losses. We concatenate the offset from the patch centers \tilde{c} , the body model parameters (pose, shape, expression) \tilde{x} , following [13, 26], and the depth \tilde{d} and minimize $\mathcal{L}_{\text{params}} = \sum_n \left| [\mathbf{c}, \mathbf{x}, d] - [\tilde{c}, \tilde{x}, \tilde{d}] \right|$. We also found it beneficial to minimize an L_1 loss for human-centered output meshes $\mathcal{L}_{\text{mesh}} = \sum_n |\mathbf{M}_n - \tilde{\mathbf{M}}_n|$, as well as for the reprojection of the mesh onto the image plane $\mathcal{L}_{\text{reproj}} = \sum_n |\pi_K(\mathbf{M}_n + \mathbf{t}_n) - \pi_K(\tilde{\mathbf{M}}_n + \tilde{\mathbf{t}}_n)|$. The final training loss is thus:

$$\mathcal{L} = \mathcal{L}_{\text{det}} + \mathcal{L}_{\text{params}} + \lambda(\mathcal{L}_{\text{mesh}} + \mathcal{L}_{\text{reproj}}). \quad (8)$$

Synthetic whole-body CUFFS dataset. We introduce CUFFS, the Close-Up Frames of Full-Body Subjects dataset, designed to contain synthetic renderings of people with close-up views of full-bodies with clearly visible hands in diverse poses, see Figure 4. We render it using Blender [1] synthetic human models close to the camera in poses sampled from BEDLAM [5], AGORA [42], and UBody [28] datasets, using additional hand poses from InterHand [37] for increased diversity. Please refer to the supplementary material for



Figure 4: Samples from our CUFFS dataset.

more details. We render a total of 60k images. Simply adding this data to the training improves the quality of hand pose predictions, without degrading other metrics.

Implementation details. By default, we use squared input images of resolution 448×448 , with the longest side resized to 448 and the smallest zero-padded to maintain aspect ratio and random horizontal flipping as data augmentation. We initialize the weights of the backbone with DINOv2 [41] and experiment with Small, Base and Large ViT models as encoder. Please refer to Appendix A.1 for the full list of hyper-parameters and more implementation details.

4. Experiments

We first perform ablation studies on training data and model architecture for single-shot whole-body HMR in Section 4.1 as well as representations and losses in Section 4.2. We then compare to the state of the art on body-only and whole-body HMR in Section 4.3.

Evaluation metrics. We evaluate the accuracy of the entire 3D mesh with the per-vertex error (PVE), following standard practice [28, 53, 54], and also measure it for specific body parts (hands and face). When the entire ground-truth mesh is not available, we report the Mean Per Joint Position Error (MPJPE) and the Percentage of Correct Keypoints (PCK) using a threshold of 15 cm. We also report these metrics after Procrustes-Alignment (PA), and F1-Scores to evaluate detection. To evaluate the placement in the scene, we report the Mean

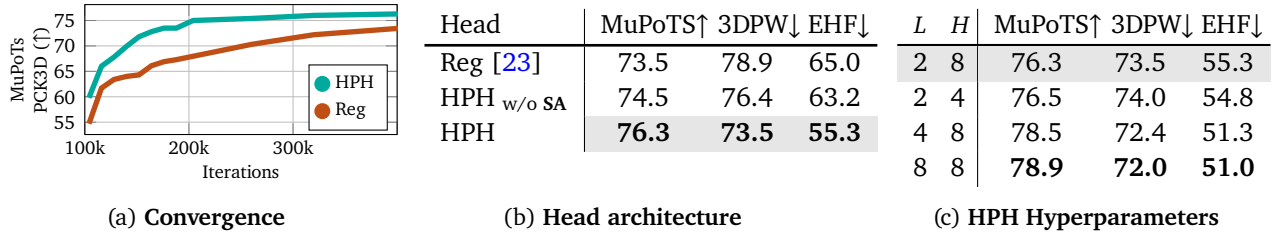


Table 3: **Ablation on the Human Perception Head (HPH)**. Reg: parallel iterative regressors; HPH w/o SA: queries processed independently in HPH, *i.e.*, without self-attention, L : number of layers and H : number of heads. (a) Training convergence speed. (b) Performance gains regarding the head choice. (c) Performance of the HPH for different hyperparameters.

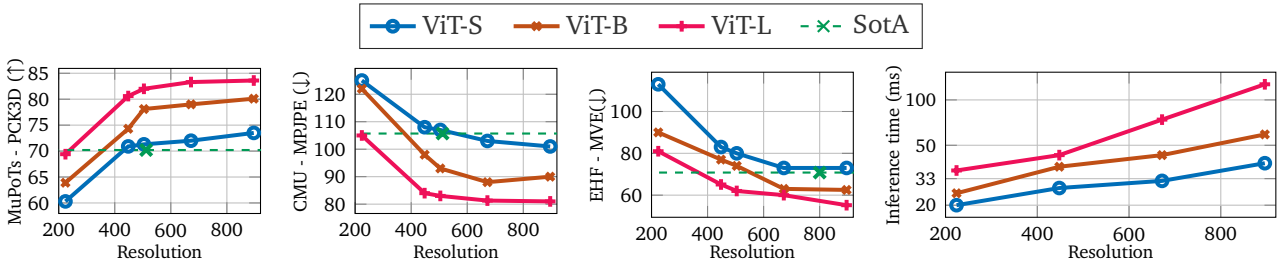


Figure 5: **Backbone-resolution-speed trade-off**. We report the performance on MuPoTs, CMU and EHF using different backbone sizes and image resolutions. We also report the inference time (right)

Root Position Error (MRPE) [54] and the Percentage of Correct Ordinal Depth (PCOD) [64] metrics. For measuring computational costs, we report inference time on a NVIDIA V100-32G GPU and the number of Multiply-Add Cumulation (MACs) using *fvcore* library¹. More details about the metrics can be found in Appendix A.

Evaluation benchmarks. For body-only benchmarks, we predict SMPL meshes from SMPL-X meshes using the regressor from [5], and follow prior work [28, 39, 45, 53, 54] in evaluating on 3DPW [57], MuPoTs [32], CMU [21] and AGORA [42]. For whole-body evaluation, we compare performance with prior work [12, 28, 39] on EHF [43], AGORA [42] and UBody [28]. We refer to Appendix A for more details on datasets.

4.1. Ablations on data and architecture

We first describe the default configuration and then evaluate the impact of the architecture in terms of backbones (including HRNet and ViTs of different sizes and resolutions) and heads, as well as the impact of training data.

Default configuration. For the ablations, we use a ViT-B as backbone by default, with 2 blocks in the HPH head, and using synthetic data for training (namely the BEDLAM and AGORA datasets, but not our proposed CUFFS dataset), and without considering the intrinsic

as input. In each table, we indicate with a grey background the default configuration of the ablations.

Model architecture. We investigate several architectures in Table 2a. As most state-of-the-art single-shot methods use a HRNet [58] convolutional backbone (ROMP [53], BEV [54], PSVT [45]), we ablate the backbone architecture by comparing HRNet with ViT-S (as they have approximately equivalent parameter counts, 28.6M for HRNet and 21M for ViT-S) with either a vanilla iterative regression head (Reg.) or our proposed HPH. In both cases, the ViT-S backbone is beneficial but significant gains also come from our proposed HPH head. Scaling up the backbone (last row) further improves performance.

Training data. In Table 2b, we experiment with different types of training data. One source can be real-world datasets (‘Real’: MS-CoCo [29], MPII [4] and Human3.6M [18]), for which pseudo-ground-truth fits [38, 40] are obtained by minimizing the reprojection error of annotated 2D keypoints, but this remains inherently noisy. An alternative is to train on synthetic datasets such as AGORA [42] (‘A’) or BEDLAM [5] (‘B’) that have the advantage to be highly scalable and to have perfect ground-truth. Recent work [5] has shown state-of-the-art results can be achieved by training only synthetics despite an inherent sim-to-real gap. Our results confirm this finding as we obtain better results when training on large-scale synthetic data. When we add our synthetic

¹<https://github.com/facebookresearch/fvcore>

	MuPoTS \uparrow 3DPW \downarrow EHF \downarrow			MuPoTS \uparrow 3DPW \downarrow EHF \downarrow			MuPoTS \uparrow 3DPW \downarrow EHF \downarrow			FOV		Reconstruction \downarrow			Distance \downarrow					
	head	76.3	74.4	55.3	v3d	75.0	76.1	65.0	none	76.3	73.5	55.3	Train	Test	MuPoTs	3DPW	CMU	MuPoTs	3DPW	CMU
	pelvis	77.0	74.5	57.5	rot	70.1	92.2	97.9	simple	74.8	75.3	56.8	60°	60°	76.3	73.5	97.2	1345	732	570
	spine1	77.1	74.9	56.1	+v3d	76.3	73.5	55.3	rays	77.0	72.6	54.4	gt	60°	76.8	76.8	99.5	1512	731	595
	spine3	76.5	74.8	56.8	+v2d	79.2	70.5	53.2	rays+ \hat{f}	78.8	71.3	53.1	gt	gt	76.5	73.2	96.9	693	445	287

(a) Primary keypoint

(b) Losses

(c) Camera embed.

(d) Impact of optional intrinsics

Table 4: **Ablative study.** We conduct ablation experiments on various aspects of Multi-HMR, including (a) the determination of the primary keypoint, (b) the influence of training losses, (c) the importance of the camera embedding type and (d) the sensitivity to the camera intrinsics in terms of human-centric reconstruction error and distance estimation error. \hat{f} : focal length normalization



Figure 6: **Randomly sampled qualitative examples** with the input image and our results overlaid on it. Images from EHF and AGORA (top), MuPoTs and 3DPW (middle), UBody and CMU (bottom). See the supplementary material for more visualizations and other views.

CUFFS dataset (‘C’) we observe a significant boost in performance especially for metrics related to the hands (column EHF-H in the third row). However, when combining both real-world and synthetic datasets (last row), performance drops compared to training solely on synthetic data (penultimate row).

HPH architecture. In Table 3, we further compare different heads to regress the SMPL-X parameters. The baseline (‘Reg.’) uses a vanilla iterative regressor [26] applied to each detected feature token independently. ‘HPH’ converges faster (Table 3a) and performs better (Table 3b). ‘HPH w/o SA’ denotes a variant where queries are treated independently by removing SA blocks from the HPH, see Equation 5: treating queries together is beneficial (Table 3b). In Table 3c we experiment with different configurations of the HPH (number of layers ‘L’ and number of attention heads ‘H’). Increasing the depth slightly improves performance but we maintain a depth of 2 for better efficiency.

Input resolution and backbone size. We empirically evaluate the impact of the input image resolution on the final performance for different backbone sizes (ViT-S, ViT-B, ViT-L) in Figure 5. Increasing the input resolution consistently brings performance gains across backbone sizes, at the cost of increased inference time (right). A ViT-L backbone at 448×448 inputs arguably offers a good performance vs. speed trade-off for body-only metrics, while using higher resolutions may be more worthwhile for whole-body metrics. We also experimented with different pre-training methods and found DINOv2 [41] consistently outperforms the others, see the supplementary material for details. The largest backbone (ViT-L) at a 896×896 resolution takes approximately 120ms per image – without compressing or quantizing the network – which is fast compared to multi-stage methods (see Section 4.3).

Method	Single shot	3DPW			MuPoTs		CMU Panoptic – MPJPE					AGORA-leaderboard		
		PA-MPJPE↓	MRJPE↓	PVE↓	PCK-All↑	PCK-Matched↑	Haggl.↓	Mafia↓	Ultim↓	Pizza↓	Mean↓	F1-Score↑	MPJPE↓	PVE↓
CRMH [20]	✓	-	-	-	69.1	72.2	129.6	133.5	153.0	156.7	143.2	-	-	-
3DCrowdNet [20]		51.5	81.7	98.3	72.7	73.3	109.6	135.9	129.8	135.6	127.3	-	-	-
ROMP [53]	✓	47.3	76.6	93.4	69.9	72.2	110.8	122.8	141.6	137.6	128.2	0.91	108.1	103.4
BEV [54]	✓	46.9	78.5	92.3	70.2	75.2	90.7	103.7	113.1	125.2	109.5	0.93	105.3	100.7
PSVT [54]	✓	45.7	75.5	84.9	-	-	88.7	97.9	115.2	121.2	105.7	0.93	97.7	94.1
Multi-HMR-448	✓	43.8	63.6	79.7	80.6	88.5	73.6	82.0	90.2	90.3	84.0	-	-	-
Multi-HMR	✓	41.7	61.4	75.9	85.0	89.3	67.3	78.6	82.1	81.0	77.3	0.93	82.8	77.6

(a) **Body-only benchmarks.** Methods other than Multi-HMR do not predict hands and facial poses.

Method	Single shot	EHF						AGORA-leaderboard			UBody-intra					
		PVE↓			PA-PVE↓			PVE↓			PVE↓			PA-PVE↓		
		All	Hands	Face	All	Hands	Face	All	Hands	Face	All	Hands	Face	All	Hands	Face
ExPose [8]		77.1	51.6	35.0	54.5	12.8	5.8	217.3	73.1	51.1	-	-	-	-	-	-
FranckMocap [50]		107.6	42.8	-	57.5	12.6	-	-	55.2	-	-	-	-	-	-	-
PIXIE [12]		89.2	42.8	32.7	55.0	11.1	4.6	191.8	49.3	50.2	168.4	55.6	45.2	61.7	12.2	4.2
Hand4Whole [39]		76.8	39.8	26.1	50.3	10.8	5.8	135.5	47.2	41.6	104.1	45.7	27.0	44.8	8.9	2.8
OSX [28]		70.8	53.7	26.4	48.7	15.9	6.0	122.8	45.7	36.2	81.9	41.5	21.2	42.2	8.6	2.0
Multi-HMR	✓	44.2	36.4	22.9	32.7	12.5	5.5	109.3	52.8	30.1	56.4	24.9	19.3	23.6	7.0	1.8

(b) **Whole-body benchmarks.** Methods other than Multi-HMR do not handle multiple humans or 3D location in scenes.

Table 5: **Comparison with state-of-the-art methods on Human Mesh Recovery benchmarks.** As there is no other method that is both multi-person and whole-body, we compare separately to state-of-the-art approaches for (a) multi-person body-only mesh recovery, and (b) whole-body mesh recovery (all methods except Multi-HMR are single-person). ■ ■ ■ methods ranked by shades of red. Note that Multi-HMR uses a ViT-L as backbone with resolution 896×896 . Multi-HMR-448 has the same backbone but image resolution is 448×448 .

4.2. Ablations on representations and losses

Primary keypoint. In Table 4a, we report results with different choices of primary keypoint: *head*, *pelvis* or *spine*. The method appears robust to this choice, though using the head as primary keypoint yields better results by a small margin. We keep the head as primary keypoint, also because it is the most often visible.

Losses on 3D and 2D. We experiment with different combinations of reconstruction losses: directly on the SMPL-X parameters (*rot*), on the vertices produced by the SMPL-X model (*v3d*), a combination of both (*rot + v3d*), and the addition of reprojection losses (*+v2d*). Table 4b shows that adding as much supervision as possible (in 3D, 2D and rotation space) yields the best performance, possibly because it reduces ambiguities during training.

Optional camera intrinsics. Integrating camera information is expected to improve accuracy when recovering and placing human 3D meshes in the scene. In Table 4c, we report results with different kinds of camera embeddings: computing *simple* embedding (where the flattening intrinsics matrix is fed to a linear layer) degrades performances compared to not adding camera embedding (*i.e.*, *none*) while adding *rays* brings a gain. When combined with focal length normalization \hat{f} , we observe a clear gain on all metrics. In Table 4d we report: performance with fixed field of view (FOV) of 60° , like ROMP/BEV, for a model trained with intrinsics (line 1), and for a model trained without (line 2).

Conditioning the model on camera intrinsics improves depth prediction accuracy (line 3), while metrics which are centered on people are far less sensitive to this change. This validates the benefit of using intrinsics when available.

4.3. Comparisons with the state of the art

None existing method is both multi-person and whole-body (Table 1). We thus compare either to multi-person approaches on body-only mesh recovery or to whole-body approaches. However, in our case, we obtain our results from the full image, while other methods assume human detections and process crops around each person. We report two settings with a ViT-L backbone: image resolution of 896×896 , which yields our best performances, and of 448×448 for SMPL benchmarks, denoted Multi-HMR-448, as it offers a good speed-performance trade-off and is more comparable to existing methods [45, 53, 54] which use 512×512 images. We show visualizations of some predictions in Figure 6.

Body Mesh Recovery. We compare against multi-person state-of-the-art methods such as ROMP [53], BEV [54] and PSVT [45], in Table 5a. All these multi-person approaches are limited to body-only meshes. Our model outperforms existing work, with substantial gains across various metrics. We conclude that Multi-HMR performs well in multi-person body-only mesh recovery. At the same time, it also predicts poses for

Method	MRPE (\downarrow)				PCOD (\uparrow)		Method	SMPL-X	Params (M)	Time (ms)			MACs (G)		
	MuPoTs	3DPW	CMU	AGORA	MuPoTs	CMU				N=1	N=5	N=10	N=1	N=5	N=10
XNect [33]	639	-	-	-	-	-	ROMP [53]		29.0	32.1	33.5	34.8	43.0	43.6	44.2
ROMP [53]	1688	1060	679	-	91.2	97.1	BEV [54]		35.8	36.6	37.8	39.1	48.6	48.9	49.9
BEV [54]	1884	1030	673	518	91.3	91.2	Hand4Whole [39] ✓		77.9	73.3	366.5	733.0	26.3	98.3	188.3
Multi-HMR							OSX [28] ✓		102.9	54.6	273.5	546.0	94.8	440.8	873.5
w/o cam.	1125	522	355	421	95.1	98.5	Multi-HMR-S ✓		32.4	28.0	28.6	28.8	44.4	44.5	44.6
w/ cam.	514	318	110	396	97.9	99.5	Multi-HMR-B ✓		99.0	38.0	38.9	39.0	143.9	144.2	144.4
							Multi-HMR-L ✓		318.7	50.8	50.9	50.9	478.7	479.5	479.8

(a) Human depth estimation benchmark

(b) Inference time and MACs

Table 6: **Comparison to existing works for human depth estimation and in terms of inference cost. (a)** Comparison to state of the art for human depth estimation. We evaluate Multi-HMR without and with camera embeddings. **(b)** Comparison of inference cost for Multi-HMR with different backbones and for the state of the art (that is limited to either multi-person but body-only methods, or single-person whole-body approaches that thus require a human detector).

faces and hands (as evaluated next), which is not the case for other multi-person approaches.

Whole-Body Mesh Recovery. We evaluate our whole-body regression performance by comparing it against whole-body 3D pose methods [12, 28, 39]. All existing approaches are limited to the single-person scenario: they do not consider the detection stage and the 3D positions in the scene, instead assuming predefined 2D bounding boxes around the person of interest. We report results in Table 5b. Multi-HMR is competitive with, or outperforms, previous whole-body methods. In particular it obtains competitive performance on hands and faces, (on par with or better than OSX [28], that is not single shot). While it performs best for the whole mesh and the face on AGORA, Multi-HMR is less precise for hands. We hypothesize that this is because AGORA has an initial 4K resolution and people are seen from afar; this may favor multi-crop approaches [28, 39], which explicitly take high-resolution crops of small body parts such as hands, whereas our method takes a single down-sampled version of the whole image. Overall, empirical results show that Multi-HMR predicts accurate hand and facial poses while also being multi-person. Note that while our model uses camera intrinsics (when available, which is not the case for the AGORA test set) in contrast to state-of-the-art methods, we have shown in Table 4d that this does not impact reconstruction metrics, ensuring a fair comparison.

Human depth estimation. In Table 6a, we compare the performance of our model in distance estimation, which uses simple depth regression, to the state of the art [33, 53, 54]. Prior works assume a fixed camera setting. For example, BEV [54] is competitive on AGORA-val but does not generalize as well to datasets with different cameras. The camera-aware variant of Multi-HMR provides accurate distance predictions across datasets and camera parameters (focal, principal point). However,

without known intrinsics, the gap with the state of the art remains significant.

Inference cost. The number N of humans only changes the number of queries to the head (HPH). With $N = 512$, HPH takes 2.5ms vs. 2.3ms for $N = 5$. The rest of the model is independent of N , thus our model scales well, see Table 6b, as other single-shot methods (e.g. ROMP, BEV) do. This is in contrast to multi-stage approaches (e.g. Hand4Whole, OSX) which detect humans (e.g. with YOLOv5) and independently process their crops. Metrics are computed for $N = \{1, 5, 10\}$.

5. Conclusion

We presented Multi-HMR, the first single-shot method for multi-person whole-body human mesh recovery. Our experiments showed that it estimates accurate expressive 3D meshes (body, face and hands) and 3D positions in the scene, outperforming the state of the art for each sub-problem. We also showed that Multi-HMR benefits from being able to adapt to camera information (i.e., intrinsics) when available. Multi-HMR is conceptually simple: it relies on a vanilla ViT architecture for the backbone, and so stands to benefit from improvements made by the broader vision community with minimal effort. Finally, while large backbones achieve the best performance, we show that using a small backbone is sufficient to achieve competitive performance and allows real-time inference.

References

- [1] Blender. <https://www.blender.org/>. 6, 15
- [2] Humgen3d. <https://www.humgen3d.com/>. 15
- [3] Poly haven. <https://polyhaven.com/>. 15
- [4] Mykhaylo Andriluka, Leonid Pishchulin, Peter Gehler, and Bernt Schiele. 2D human pose estimation: New benchmark and state of the art analysis. In *CVPR*, 2014.

7

- [5] Michael J. Black, Priyanka Patel, Joachim Tesch, and Jinlong Yang. BEDLAM: A synthetic dataset of bodies exhibiting detailed lifelike animated motion. In *CVPR*, 2023. 2, 4, 6, 7, 14, 15
- [6] Mathilde Caron, Hugo Touvron, Ishan Misra, Hervé Jégou, Julien Mairal, Piotr Bojanowski, and Armand Joulin. Emerging properties in self-supervised vision transformers. In *ICCV*, 2021. 2, 16
- [7] Hongsuk Choi, Gyeongsik Moon, JoonKyu Park, and Kyoung Mu Lee. Learning to estimate robust 3d human mesh from in-the-wild crowded scenes. In *CVPR*, 2022. 2, 3
- [8] Vasileios Choutas, Georgios Pavlakos, Timo Bolkart, Dimitrios Tzionas, and Michael J Black. Monocular expressive body regression through body-driven attention. In *ECCV*, 2020. 2, 3, 4, 9
- [9] Agostino De Santis, Bruno Siciliano, Alessandro De Luca, and Antonio Bicchi. An atlas of physical human-robot interaction. *Mechanism and Machine Theory*, 2008. 2
- [10] Alexey Dosovitskiy, Lucas Beyer, Alexander Kolesnikov, Dirk Weissenborn, Xiaohua Zhai, Thomas Unterthiner, Mostafa Dehghani, Matthias Minderer, Georg Heigold, Sylvain Gelly, et al. An image is worth 16x16 words: Transformers for image recognition at scale. In *ICLR*, 2021. 2, 4
- [11] Jose M Facil, Benjamin Ummenhofer, Huizhong Zhou, Luis Montesano, Thomas Brox, and Javier Civera. Cam-convs: Camera-aware multi-scale convolutions for single-view depth. In *CVPR*, 2019. 5
- [12] Yao Feng, Vasileios Choutas, Timo Bolkart, Dimitrios Tzionas, and Michael J Black. Collaborative regression of expressive bodies using moderation. In *3DV*, 2021. 2, 3, 7, 9, 10, 16, 19
- [13] Shubham Goel, Georgios Pavlakos, Jathushan Rajasegaran, Angjoo Kanazawa, and Jitendra Malik. Humans in 4d: Reconstructing and tracking humans with transformers. In *ICCV*, 2023. 2, 3, 5, 6, 17
- [14] Yana Hasson, Gül Varol, Dimitrios Tzionas, Igor Kalevatykh, Michael J. Black, Ivan Laptev, and Cordelia Schmid. Learning joint reconstruction of hands and manipulated objects. In *CVPR*, 2019. 4
- [15] Kaiming He, Georgia Gkioxari, Piotr Dollár, and Ross Girshick. Mask r-cnn. In *CVPR*, 2017. 3
- [16] Kaiming He, Xinlei Chen, Saining Xie, Yanghao Li, Piotr Dollár, and Ross Girshick. Masked autoencoders are scalable vision learners. In *CVPR*, 2022. 2
- [17] Buzhen Huang, Tianshu Zhang, and Yangang Wang. Pose2uv: Single-shot multi-person mesh recovery with deep uv prior. *IEEE trans. Image Processing*, 2022. 16, 19
- [18] Catalin Ionescu, Dragos Papava, Vlad Olaru, and Cristian Sminchisescu. Human3.6M: Large scale datasets and predictive methods for 3D human sensing in natural environments. *IEEE trans. PAMI*, 2013. 7
- [19] Andrew Jaegle, Felix Gimeno, Andy Brock, Oriol Vinyals, Andrew Zisserman, and Joao Carreira. Perceiver: General perception with iterative attention. In *ICML*, 2021. 5
- [20] Wen Jiang, Nikos Kolotouros, Georgios Pavlakos, Xiaowei Zhou, and Kostas Daniilidis. Coherent reconstruction of multiple humans from a single image. In *CVPR*, 2020. 9, 14
- [21] Hanbyul Joo, Hao Liu, Lei Tan, Lin Gui, Bart Nabbe, Iain Matthews, Takeo Kanade, Shohei Nobuhara, and Yaser Sheikh. Panoptic studio: A massively multiview system for social motion capture. In *ICCV*, 2015. 3, 7, 14
- [22] Hanbyul Joo, Natalia Neverova, and Andrea Vedaldi. Exemplar fine-tuning for 3d human pose fitting towards in-the-wild 3d human pose estimation. In *3DV*, 2020. 2
- [23] Angjoo Kanazawa, Michael J. Black, David W. Jacobs, and Jitendra Malik. End-to-end recovery of human shape and pose. In *CVPR*, 2018. 2, 6, 7
- [24] Jeonghwan Kim, Mi-Gyeong Gwon, Hyunwoo Park, Hyukmin Kwon, Gi-Mun Um, and Wonjun Kim. Sampling is matter: Point-guided 3d human mesh reconstruction. In *CVPR*, 2023. 3
- [25] Muhammed Kocabas, Chun-Hao P Huang, Joachim Tesch, Lea Müller, Otmar Hilliges, and Michael J Black. Spec: Seeing people in the wild with an estimated camera. In *ICCV*, 2021. 2
- [26] Nikos Kolotouros, Georgios Pavlakos, Michael J Black, and Kostas Daniilidis. Learning to reconstruct 3d human pose and shape via model-fitting in the loop. In *ICCV*, 2019. 2, 3, 5, 6, 8, 14, 17
- [27] Zhihao Li, Jianzhuang Liu, Zhensong Zhang, Songcen Xu, and Youliang Yan. Cliff: Carrying location information in full frames into human pose and shape estimation. In *ECCV*, 2022. 2, 14, 16, 19
- [28] Jing Lin, Ailing Zeng, Haoqian Wang, Lei Zhang, and Yu Li. One-stage 3d whole-body mesh recovery with component aware transformer. In *CVPR*, 2023. 2, 3, 6, 7, 9, 10, 14
- [29] Tsung-Yi Lin, Michael Maire, Serge Belongie, James Hays, Pietro Perona, Deva Ramanan, Piotr Dollár, and C Lawrence Zitnick. Microsoft coco: Common objects in context. In *ECCV*, 2014. 7
- [30] Wei Liu, Dragomir Anguelov, Dumitru Erhan, Christian Szegedy, Scott Reed, Cheng-Yang Fu, and Alexander C Berg. Ssd: Single shot multibox detector. In *ECCV*, 2016. 3
- [31] Xiaoxuan Ma, Jiajun Su, Chunyu Wang, Wentao Zhu, and Yizhou Wang. 3d human mesh estimation from virtual markers. In *CVPR*, 2023. 3
- [32] Dushyant Mehta, Oleksandr Sotnychenko, Franziska Mueller, Weipeng Xu, Srinath Sridhar, Gerard Pons-Moll, and Christian Theobalt. Single-shot multi-person 3d pose estimation from monocular rgb. In *3DV*, 2018. 3, 7, 14
- [33] Dushyant Mehta, Oleksandr Sotnychenko, Franziska Mueller, Weipeng Xu, Mohamed Elgharib, Pascal Fua,

- Hans-Peter Seidel, Helge Rhodin, Gerard Pons-Moll, and Christian Theobalt. Xnect: Real-time multi-person 3d motion capture with a single rgb camera. *ACM trans. Graph.*, 2020. 10
- [34] Alican Mertan, Damien Jade Duff, and Gozde Unal. Single image depth estimation: An overview. *Digital Signal Processing*, 2022. 5
- [35] Paulius Micikevicius, Sharan Narang, Jonah Alben, Gregory Diamos, Erich Elsen, David Garcia, Boris Ginsburg, Michael Houston, Oleksii Kuchaiev, Ganesh Venkatesh, et al. Mixed precision training. In *ICLR*, 2018. 14
- [36] Ben Mildenhall, Pratul P. Srinivasan, Matthew Tancik, Jonathan T. Barron, Ravi Ramamoorthi, and Ren Ng. Nerf: Representing scenes as neural radiance fields for view synthesis. In *ECCV*, 2020. 5
- [37] Gyeongsik Moon, Shoou-I Yu, He Wen, Takaaki Shiratori, and Kyoung Mu Lee. Interhand2. 6m: A dataset and baseline for 3d interacting hand pose estimation from a single rgb image. In *ECCV*, 2020. 6, 15
- [38] Gyeongsik Moon, Hongsuk Choi, and Kyoung Mu Lee. Neuralannot: Neural annotator for 3d human mesh training sets. In *CVPR Workshop*, 2022. 7
- [39] Gyeongsik Moon, Hongsuk Choi, and Kyoung Mu Lee. Accurate 3d hand pose estimation for whole-body 3d human mesh estimation. In *CVPR Workshop*, 2022. 2, 3, 7, 9, 10
- [40] Gyeongsik Moon, Hongsuk Choi, Sanghyuk Chun, Jiyoung Lee, and Sangdoo Yun. Three recipes for better 3d pseudo-gts of 3d human mesh estimation in the wild. In *CVPR Workshop*, 2023. 7
- [41] Maxime Oquab, Timothée Darcet, Theo Moutakanni, Huy V. Vo, Marc Szafraniec, Vasil Khalidov, Pierre Fernandez, Daniel Haziza, Francisco Massa, Alaaeldin El-Nouby, Russell Howes, Po-Yao Huang, Hu Xu, Vasu Sharma, Shang-Wen Li, Wojciech Galuba, Mike Rabbat, Mido Assran, Nicolas Ballas, Gabriel Synnaeve, Ishan Misra, Herve Jegou, Julien Mairal, Patrick Labatut, Armand Joulin, and Piotr Bojanowski. Dinov2: Learning robust visual features without supervision. *TMLR*, 2023. 2, 6, 8, 14, 16
- [42] Priyanka Patel, Chun-Hao P Huang, Joachim Tesch, David T Hoffmann, Shashank Tripathi, and Michael J Black. AGORA: Avatars in geography optimized for regression analysis. In *CVPR*, 2021. 2, 3, 4, 6, 7, 14, 15
- [43] Georgios Pavlakos, Vasileios Choutas, Nima Ghorbani, Timo Bolkart, Ahmed AA Osman, Dimitrios Tzionas, and Michael J Black. Expressive body capture: 3d hands, face, and body from a single image. In *CVPR*, 2019. 2, 3, 7, 14
- [44] Zhongwei Qiu, Qiansheng Yang, Jian Wang, and Dongmei Fu. Dynamic graph reasoning for multi-person 3d pose estimation. In *ACMMM*, 2022. 3
- [45] Zhongwei Qiu, Qiansheng Yang, Jian Wang, Haocheng Feng, Junyu Han, Errui Ding, Chang Xu, Dongmei Fu, and Jingdong Wang. Psvt: End-to-end multi-person 3d pose and shape estimation with progressive video transformers. In *CVPR*, 2023. 2, 3, 7, 9, 14
- [46] Jathushan Rajasegaran, Georgios Pavlakos, Angjoo Kanazawa, and Jitendra Malik. Tracking people by predicting 3d appearance, location and pose. In *CVPR*, 2022. 5
- [47] Jathushan Rajasegaran, Georgios Pavlakos, Angjoo Kanazawa, Christoph Feichtenhofer, and Jitendra Malik. On the benefits of 3d pose and tracking for human action recognition. In *CVPR*, 2023. 2
- [48] Joseph Redmon, Santosh Divvala, Ross Girshick, and Ali Farhadi. You only look once: Unified, real-time object detection. In *CVPR*, 2016. 3
- [49] Javier Romero, Dimitrios Tzionas, and Michael J Black. Embodied hands: Modeling and capturing hands and bodies together. *ACM trans. Graph.*, 2017. 15
- [50] Yu Rong, Takaaki Shiratori, and Hanbyul Joo. Frankmcap: A monocular 3d whole-body pose estimation system via regression and integration. In *ICCV*, 2021. 3, 9
- [51] Tim Salzman, Hao-Tien Lewis Chiang, Markus Ryll, Dorsa Sadigh, Carolina Parada, and Alex Bewley. Robots that can see: Leveraging human pose for trajectory prediction. *IEEE RAL*, 2023. 2
- [52] Anshul Shah, Shlok Mishra, Ankan Bansal, Jun-Cheng Chen, Rama Chellappa, and Abhinav Shrivastava. Pose and joint-aware action recognition. In *WACV*, 2022. 2
- [53] Yu Sun, Qian Bao, Wu Liu, Yili Fu, Michael J Black, and Tao Mei. Monocular, one-stage, regression of multiple 3d people. In *ICCV*, 2021. 2, 3, 6, 7, 9, 10, 14, 19
- [54] Yu Sun, Wu Liu, Qian Bao, Yili Fu, Tao Mei, and Michael J Black. Putting people in their place: Monocular regression of 3d people in depth. In *CVPR*, 2022. 2, 3, 5, 6, 7, 9, 10, 14
- [55] Omid Taheri, Nima Ghorbani, Michael J. Black, and Dimitrios Tzionas. GRAB: A dataset of whole-body human grasping of objects. In *ECCV*, 2020. 15
- [56] Gül Varol, Javier Romero, Xavier Martin, Naureen Mahmood, Michael J. Black, Ivan Laptev, and Cordelia Schmid. Learning from synthetic humans. In *CVPR*, 2017. 4
- [57] Timo von Marcard, Roberto Henschel, Michael Black, Bodo Rosenhahn, and Gerard Pons-Moll. Recovering accurate 3d human pose in the wild using imus and a moving camera. In *ECCV*, 2018. 3, 7, 14
- [58] Jingdong Wang, Ke Sun, Tianheng Cheng, Borui Jiang, Chaorui Deng, Yang Zhao, Dong Liu, Yadong Mu, Mingkui Tan, Xinggang Wang, et al. Deep high-resolution representation learning for visual recognition. *IEEE trans. PAMI*, 2020. 7
- [59] Philippe Weinzaepfel, Thomas Lucas, Vincent Leroy, Johann Cabon, Vaibhav Arora, Romain Brégier, Gabriela Csurka, Leonid Antsfeld, Boris Chidlovskii, and Jérôme Revaud. CroCo v2: Improved cross-view completion pre-training for stereo matching and optical flow. In *ICCV*, 2023. 5
- [60] Yufei Xu, Jing Zhang, Qiming Zhang, and Dacheng Tao. ViTPose: Simple vision transformer baselines for human pose estimation. In *NeurIPS*, 2022. 17

- [61] Zhitao Yang, Zhongang Cai, Haiyi Mei, Shuai Liu, Zhaoxi Chen, Weiye Xiao, Yukun Wei, Zhongfei Qing, Chen Wei, Bo Dai, Wayne Wu, Chen Qian, Dahua Lin, Ziwei Liu, and Lei Yang. Synbody: Synthetic dataset with layered human models for 3d human perception and modeling. In *ICCV*, 2023. [4](#)
- [62] Yusuke Yoshiyasu. Deformable mesh transformer for 3d human mesh recovery. In *CVPR*, 2023. [3](#)
- [63] Hongwen Zhang, Yating Tian, Xinchu Zhou, Wanli Ouyang, Yebin Liu, Limin Wang, and Zhenan Sun. Py-maf: 3d human pose and shape regression with pyramidal mesh alignment feedback loop. In *ICCV*, 2021. [2](#), [3](#)
- [64] Jianan Zhen, Qi Fang, Jiaming Sun, Wentao Liu, Wei Jiang, Hujun Bao, and Xiaowei Zhou. Smap: Single-shot multi-person absolute 3d pose estimation. In *ECCV*, 2020. [7](#)
- [65] Ce Zheng, Xianpeng Liu, Guo-Jun Qi, and Chen Chen. Potter: Pooling attention transformer for efficient human mesh recovery. In *CVPR*, 2023. [3](#)
- [66] Lijuan Zhou, Xiang Meng, Zhihuan Liu, Mengqi Wu, Zhimin Gao, and Pichao Wang. Human pose-based estimation, tracking and action recognition with deep learning: A survey. *arXiv preprint arXiv:2310.13039*, 2023. [2](#)
- [67] Xingyi Zhou, Dequan Wang, and Philipp Krähenbühl. Objects as points. In *arXiv preprint arXiv:1904.07850*, 2019. [2](#), [4](#), [17](#)
- [68] Yuxiao Zhou, Marc Habermann, Ikhsanul Habibie, Ayush Tewari, Christian Theobalt, and Feng Xu. Monocular real-time full body capture with inter-part correlations. In *CVPR*, 2021. [3](#)

Appendix

This appendix contains additional descriptions of the datasets and metrics used in the main paper (Appendix A), details about how we generated our synthetic CUFFS dataset (Appendix B), additional quantitative results (Appendix C) and a discussion on limitations (Appendix D).

A. Implementation, Datasets and Metrics

In this section, we give details about implementation, as well as each dataset used in the main paper, followed by a detailed description of the evaluation metrics.

A.1. Implementation details

By default, we use squared input images of resolution 448×448 , with the longest side resized to 448 and the smallest zero-padded to maintain aspect ratio. We only use random horizontal flipping as data augmentation. We initialize the weights of the backbone with DINOv2 [41]. We experiment with Small, Base and Large ViT models as encoder. We use a batch-size of 8 images, an initial learning rate of $5e-5$, train our model with automated mixed precision [35] for 400k iterations. At resolution 448×448 , training a ViT-S (resp. ViT-L) takes around 2 (resp. 5) days on a single NVIDIA V100. The default detection threshold is $\tau=0.5$. We use the neutral SMPL-X model with 10 shape components.

A.2. Datasets descriptions

BEDLAM [5] is a large-scale multi-person synthetic dataset composed of 300k images for training including diverse body shapes, skin tones, hair and clothing. Synthetic humans are built by using a SMPL-X mesh and adding some assets such as clothes and hair. In each scene there are from 1 to 10 people with diverse camera viewpoints. The test set is composed of 16k images.

AGORA [42] is a multi-person high realism synthetic dataset which contains 14k images for training, 2k images for validation and 3k for testing. It consists of 4,240 high-quality humans scans each fitted with accurate SMPL and SMPL-X annotations. Results on the test set are obtained using an online leaderboard for SMPL and SMPL-X results. We also report results on the validation for the distance estimation following [53, 54] since the leaderboard does not give this metric on the test set.

3DPW [57] is an outdoor multi-person dataset com-

posed of 60 sequences which contain respectively 17k images for training, 8k images for validation and 24k images for testing. This has been the first in-the-wild dataset in this domain for evaluating body mesh reconstruction methods [26,27].

MuPoTs [32] is an outdoor multi-person dataset captured in a multi-view setting. The dataset is composed of 8k frames from 20 real-world scenes with up to three subjects. We use this dataset for evaluation only. Poses are annotated in 3D with 14 body joints.

CMU Panoptic [21] is a large-scale controlled environment multi-person dataset captured by multiple cameras. Each person is annotated with 14 joints in 3D. Following prior works [20,45] we use 4 sequences which leads to a test set composed of 9k images.

EHF [43] is the first evaluation dataset for SMPL-X based models. It was built using a scanning system followed by a fitting of the SMPL-X mesh. It is a single person whole-body pose dataset composed of 100 images.

UBody [28] is a large-scale dataset covering a wide range of real-life scenarios such as fitness videos, VLOGs or sign language. Most of the time only the upper body part of the persons is visible. We use the inter-scene protocol where there are 55k images for training and 2k images for testing.

A.3. Metrics Descriptions

Prior work on multi-person human mesh recovery proposed metrics that can be separated into three categories: i) metrics that evaluate the reconstruction of the human mesh, centered around the root joint; ii) metrics that evaluate detection and iii) metrics that evaluate the prediction of spatial location. In this section, we review the metrics used in the main paper.

Human-centered mesh metrics. To evaluate the predicted human mesh, we center both estimated and ground-truth human meshes around the pelvis joint. We use per-vertex error (PVE) to evaluate the accuracy of the entire 3D mesh. When available, we also report PVE computed on vertices corresponding to the face and hands only (PVE-Face and PVE-Hands). Because global orientation mistakes heavily impact the PVE, we also assess prediction quality without taking the global orientation into account by reporting all these metrics after Procrustes-Alignment (denoted with the prefix PA). Since some human body datasets do not have mesh ground-truths but only 3D keypoints, we also report Mean Per Joint Position Error (MPJPE) on the 14 LSP 3D keypoints as well as the Percentage of



Figure 7: **Samples from our CUFFS dataset** with a rendered human using HumGen3D (top) and the corresponding SMPL-X shape used for retargeting (overlaid at the bottom).

Correct Keypoints (PCK) using a threshold of 15 cm.

Detection metrics. To evaluate detection we rely on the Recall, Precision and F1-Score metrics. On some datasets, it is also common to report normalized mean joints error (NMJE) and normalized mean vertex error (NMVE), which are obtained by dividing mean joint errors and mean vertex errors by the F1-Score. This produces a score sensitive to both reconstruction quality and detection.

Spatial location metrics. To evaluate distance predictions we use the Mean Root Position Error (MRPE) by using the pelvis as root keypoint.

B. The synthetic CUFFS dataset

Motivation. Existing synthetic datasets, namely BEDLAM and AGORA, provide perfect ground truths for the SMPL-X model, *i.e.*, including faces and hands. However, in these datasets: i) most humans are seen from afar, which is not ideal to capture subtle details needed to properly reconstruct faces and hands and ii) hand poses lack diversity. In particular since our method is single-shot, *i.e.*, runs without specific image crops or feature resampling around hands, hands consist of only a few visible pixels for many training images. We remedy this by adding a dedicated, booster dataset, consisting of close-up pictures of single humans with clearly visible hands in diverse poses, to the rest of the training data.

3D Human models. We render images of 3D human models. Following the strategy of BEDLAM [5], we use a procedural generation pipeline with fine control over parameters, rather than commercially available scans of clothed humans (*e.g.* as in AGORA [42]). To this end, we make use of HumGen3D [2], an open-source human generator add-on to the Blender software tool [1]. This add-on generates 3D rigged human models, with

different clothing (layered on top of the body mesh), hairstyles, skin tones, age, *etc.* This yields a high diversity of humans overall.

Retargeting with SMPL-X. In order to get precisely annotated images, we manually define pointwise correspondences between the SMPL-X and the HumGen3D meshes. For a given set of SMPL-X parameters as input, we iteratively optimize the skeleton parameters of the HumGen3D model – which control the corresponding mesh through linear blend skinning – to minimize the distance between keypoints of both meshes. Figure 7 shows examples of rendered avatars and their associated SMPL-X meshes and allows to verify the quality of the retargeting.

Rendering. Characters are placed into empty scenes so as to take up most of the space in the camera plane with random HDRIs images taken from Poly Haven [3] as environment maps. We use a focal of 843 pixels and render images with resolution 900×675 . The principal point is set at the center of the image.

Human shape sources and hand diversity. We seek to generate humans that are: i) close to the camera such that the hands are sufficiently visible, and ii) with diverse hand poses. For the first point, we simply render images of a single person, facing the camera, at a distance varying slightly around 2.5 meters. We find that this yields visible hands. For the second point, we sample human poses from BEDLAM, AGORA, and UBody, where hand annotations are respectively: taken from the GRAB [55] dataset, fitted to 3D scans, and fitted to in-the-wild images. In addition to these three sources, in order to further diversify our set of hand poses, we also augment UBody’s annotations with hands from other sources: we create a large set of diverse hand poses using MANO [49] annotations from the InterHand [37] dataset. This is done by extracting all MANO annotations and transforming hands into right-hand format. When creating a synthetic image with augmented hands, we sample two random hands from the large set, transform one into a left hand and replace hands from the chosen SMPL-X annotations using the new hand poses. This provides an even richer set of hands than the original InterHand annotations: left hands can be turned into right hands which increases the number of possible combinations.

Dataset. We generate about 73k images, equally spread with human shapes from i) BEDLAM, ii) AGORA, iii) UBody, iv) UBody with increased hand diversity. We show qualitative examples of our generated images and the associated SMPL-X mesh in Figures 7 and 8. We also provide examples of hand swapped shapes in Figure 9.

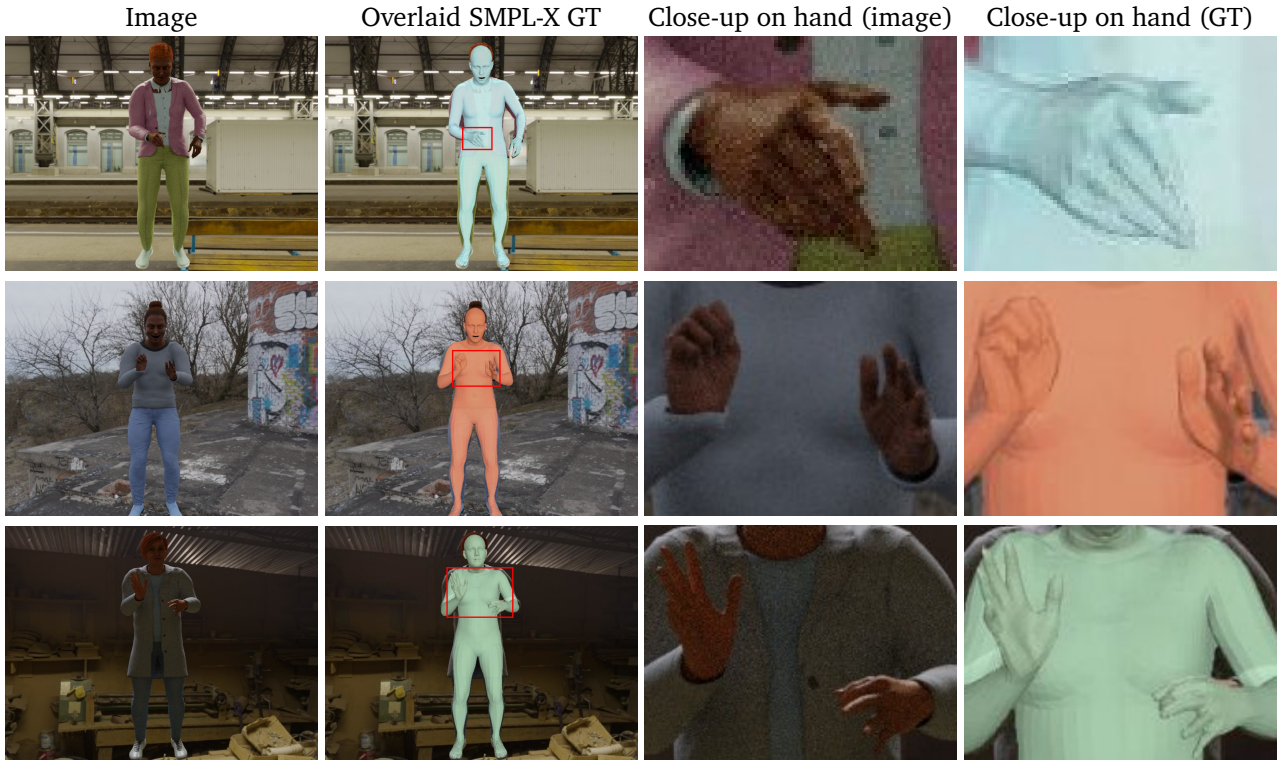


Figure 8: Examples from the CUFFS dataset showing the input image, the overlaid SMPL-X annotations, the close-up image and annotations around the hands corresponding to the rectangle shown in the second column. People are seen up close, and diverse hand poses are used.

Impact. In addition to the quantitative gain reported in the main paper, we show some qualitative example of adding the synthetic CUFFS dataset to the training set in Figure 10. For instance, in the third example, the hands are significantly better predicted when the training set includes our synthetic CUFFS dataset.

C. Additional results

We now present additional results, regarding i) results on all benchmarks obtained with a universal model, *i.e.*, without any dataset-specific finetuning, ii) results on two additional test sets (BEDLAM and 3DMPB), and finally iii) ablations on the type of pretraining used to initialize the backbone for Multi-HMR.

Universal model. In the main paper we first pre-train on synthetic data only (BEDLAM, AGORA and CUFFS) and then we follow the standard practice of finetuning independently on AGORA, 3DPW and UBody to compare to the state of the art on each benchmark. Here, we also evaluate the performance obtained with a single ‘universal’ model in Table 7 shared for all benchmarks, without finetuning on any specific dataset. The universal model is trained on a combination of BEDLAM, AGORA, CUFFS and UBody as we found that including UBody in the training data improve robustness to in-

the-wild images while not degrading (even improving on some test sets) the performance too much compared to using other real-world data such MS-CoCo or MPII. Results are reported at input resolution 896×896 using ViT-Large backbone. To achieve the best performance on a target dataset such as 3DPW or UBody with Multi-HMR, we still need to finetune on the associated train set.

Results on BEDLAM-test. We report results on BEDLAM-test in Table 8 using the recently released online leaderboard. Since the leaderboard is extremely recent (online since October 2023), we were unable to compare to many existing methods. At present, only single-person methods [12, 27] are reported in the leaderboard which makes the comparison with our method difficult. Still, Multi-HMR achieves competitive performances on this dataset.

Results on 3DMPB. We report results on whole-body predictions on the 3DMPB dataset [17] in Table 9. Multi-HMR reaches state-of-the-art performance with all backbones (ViT-S/B/L).

Backbone pretraining. In Figure 11, we report results using various pretraining methods, with a ViT-Base architecture and 448×448 input images. DINO [6] and DINOv2 [41] rely on self-supervised pre-training, while



Figure 9: **Illustrations of how we increase hand diversity in human shape sources to be rendered.** Given an annotation from UBody (image on top, annotation in the middle row), we swap the hands from a large set built from InterHand to have more diversity in terms of hand poses.

ViT-Pose [60] is trained with 2D body keypoints supervision. DINOv2 leads to the best final performance, and converges faster. The difference in performance decreases while training longer, which may be due to the relatively large size of our training set, with ViT-Pose eventually achieving comparable results. Thus, using DINOv2 may be most beneficial when training compute is limited.

D. Limitations

While Multi-HMR reaches state-of-the-art performance across multiple human mesh recovery benchmarks, we still observe some limitations that may be improved upon in the future.

Patch-level detection. We follow the CenterNet [67] paradigm for the detection stage, which allows us to propose a single-shot method without elaborate post-processing. However it comes with the main limitation that multiple humans (i.e. person-centers) may belong to the same patch in the image. Because of this, some collisions happen during training and some detections are impossible at inference time. This well-known limitation is already discussed in Appendix C of the CenterNet paper [67]. We refer reader to this section for more details. In our case we observe that as long as we use images of reasonable resolution (i.e. more than 448×448) and a small patch-size (i.e. 14×14), collisions remain very rare at training. As shown in the attached video,

Multi-HMR produces reasonable predictions even in relatively crowded environment which indicates that our modeling is robust enough. We also still think that a potential future work is to have multiple queries per patch.

Truncated humans. We observe that Multi-HMR sometimes struggles to detect humans when the head is not visible; this may in part be due to the fact that we chose the head as primary keypoint, and also to the fact that such data is very rare in the datasets. We still observe (see attached video) that Multi-HMR is able to detect human when only a small part of the head is visible. We make the assumption that adding more aggressive cropping augmentations at training time would lead to a model more robust to this type of truncation by the image frame. As shown in the attached video, we observe that Multi-HMR is already quite robust to occlusion in general.

SMPL-X representation. We employ the SMPL-X parametric 3D model for representing whole-body human mesh. As discussed in the method section, we use the pose parameters expressed by the relative rotations of each joint regarding its parent given a pre-defined kinematic tree. Such representation is easy to use and commonly relied upon in practice [13, 26], however it may raise several concerns: i) in general rotations are not easy to regress since they are not expressed in a continuous space; we use the 6D representation for regression, for which rotations are supposed to be con-

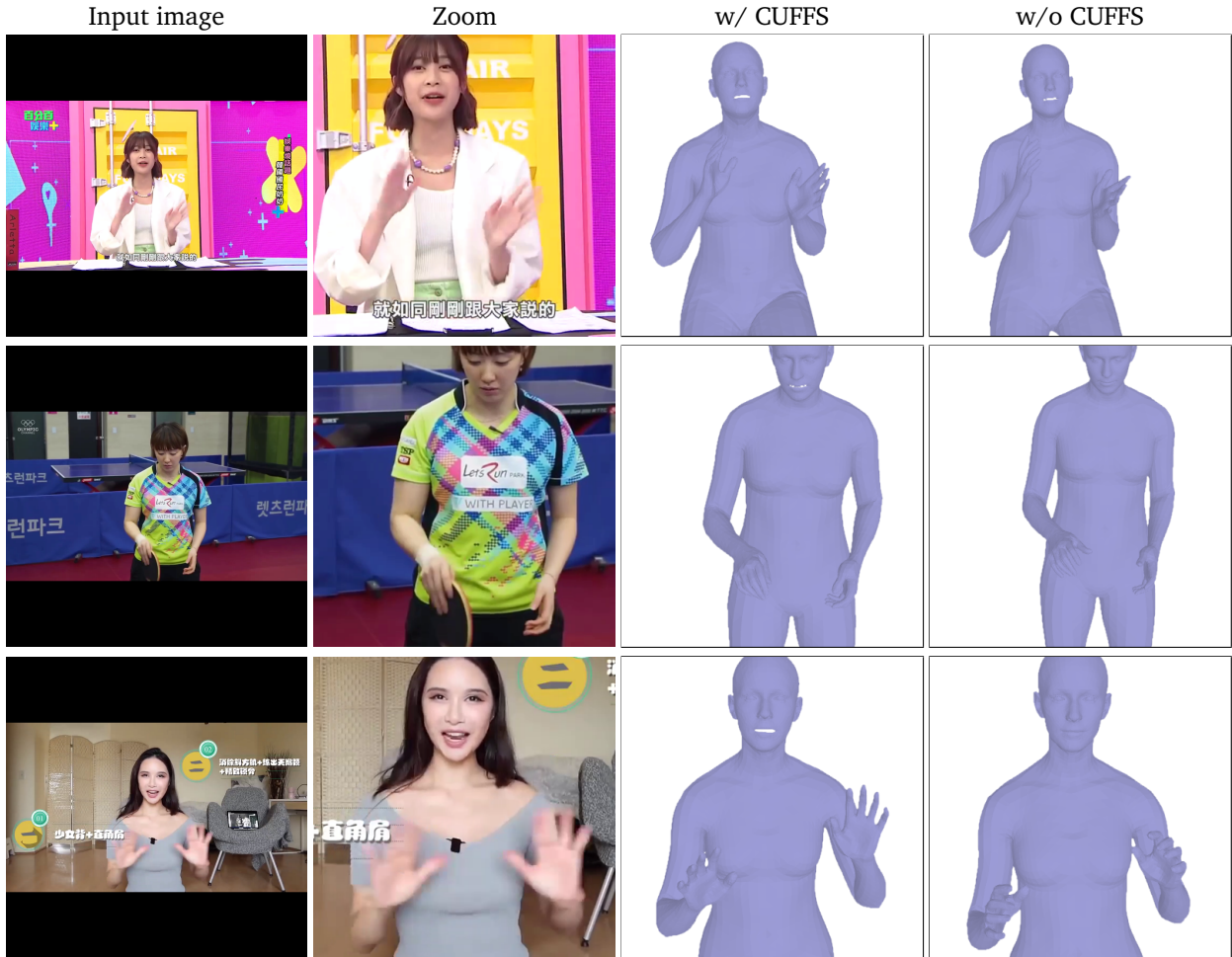


Figure 10: **Qualitative results on some UBody images with or without training with our synthetic CUFFS dataset.** Hand pose predictions are more accurate when the model has been trained with the synthetic CUFFS dataset.

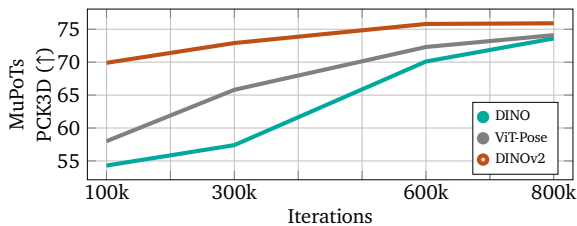


Figure 11: **Impact of backbone pretraining.** Initializing the backbone with DINOv2 leads to faster convergence.

tinuous. This is a topic that may not have been explored sufficiently in the 3D vision community so far and may deserve further work. ii) regressing the pose using a relative representation can lead to an accumulation of errors, particularly on the extreme parts of the body (hands, legs). We believe that investigating different pose representations would be beneficial for Multi-HMR and the human mesh recovery field in general.

	3DPW			MuPoTs		CMU Panoptic – MPJPE				
	PA-MPJPE↓	MPJPE↓	PVE↓	PCK-All↑	PCK-Matched↑	Haggl.↓	Mafia↓	Ultim↓	Pizza↓	Mean↓
Universal model	45.6	67.6	87.3	83.5	87.5	78.1	94.5	98.7	101.7	95.6
Finetuned model	41.7	61.4	75.9	85.0	89.3	67.3	78.6	82.1	81.0	77.3

(a) Body-only benchmarks

	EHF						UBody-intra					
	PVE↓			PA-PVE↓			PVE↓			PA-PVE↓		
	All	Hands	Face	All	Hands	Face	All	Hands	Face	All	Hands	Face
Universal model	45.4	31.0	20.0	29.4	11.8	5.4	56.9	27.9	20.2	24.0	8.5	2.4
Finetuned model	44.2	36.4	22.9	32.7	12.5	5.5	56.4	24.9	19.3	23.6	7.0	1.8

(b) Whole-body benchmarks

Table 7: **Results of Multi-HMR without and with finetuning.** The universal model (first row of each table) is trained on the combination of AGORA, BEDLAM, Ubody and CUFFS, and we report results on all benchmarks using the exact same weights. For results of the finetuning models (second row of each table), we first train on AGORA, BEDLAM and CUFFS and then finetune on the training set if it exists (*i.e.*, 3DPW, UBody). Evaluation on (a) body-only and (b) whole-body benchmarks.

Method	F1-Score↑	Precision↑	Recall↑	Body-MVE↓	FullBody-MVE↓	Face-MVE↓	LHand-MVE↓	RHand-MVE↓
PIXIE [12]	0.94	0.99	0.90	100.8	149.2	51.4	44.8	48.9
CLIFF [27]	0.94	0.99	0.90	61.3	94.6	29.8	34.7	35.5
CLIFF+ [27]	0.94	0.99	0.90	57.5	87.2	27.3	30.3	32.6
Multi-HMR	0.92	0.88	0.97	64.4	94.9	31.8	28.7	30.9

Table 8: **BEDLAM-test leaderboard.** CLIFF is trained on BEDLAM, CLIFF+ on BEDLAM+AGORA. *Multi-HMR* is the only multi-person and the only single-shot method reported on the benchmark to date.

Method	PA-MPJPE↓
ROMP [53]	72.0
Pose2UV [17]	69.5
Multi-HMR ViT-S	62.6
Multi-HMR ViT-B	55.8
Multi-HMR ViT-L	49.7

Table 9: **Comparison to the state of the art on the 3DMPB dataset.**